ACS OMEGA

http://pubs.acs.org/journal/acsodf

Article

Facile Synthesis of a Novel Ni-WO_3@g-C_3N_4 Nanocomposite for Efficient Oxidative Desulfurization of Both Model and Real Fuel

Muhammad Saeed, Mamoona Munir, Azeem Intisar, and Amir Waseem*

Cite This: *ACS Omega* 2022, 7, 15809−15820

Read Online

ACCESS | Metrics & More | Article Recommendations

ABSTRACT: The current study comprises the successful synthesis of a Ni-WO_3@g-C_3N_4 composite as an efficient and recoverable nanocatalyst for oxidative desulfurization of both model and real fuel oils. The physiochemical characterization of the synthesized composite was confirmed via Fourier transform infrared spectroscopy, X-ray diffraction, scanning electron microscopy (SEM), energy-dispersive X-ray spectroscopy, and thermogravimetric analysis. SEM results showed that Ni-WO_3 particles were well-decorated on the g-C_3N_4 surface with an interesting morphology as appeared on the surface like spherical particles. The obtained findings revealed that 97% dibenzothiophene (DBT) removal can be achieved under optimized conditions (0.1 g of the catalyst, 1 mL of an oxidant, 100 mg/L DBT-based model fuel, a time duration of 180 min, and a temperature of 40 °C). Additionally, the catalytic activity for real fuel was also investigated in which 89.5 and 91.2% removal efficiencies were achieved for diesel and kerosene, respectively, as well as fuel properties following ASTM specifications. A pseudo first-order kinetic model was followed well for this reaction system, and the negative value of ΔG was due to the spontaneous process. Additionally, the desulfurization study was optimized via a response surface methodology (RSM/Box−Behnken design) for predicting optimum removal of sulfur species by drawing three-dimensional RSM surface plots. The Ni-WO_3@g-C_3N_4 proved to be a promising catalyst for desulfurization of fuel oil by exhibiting reusability of five times with no momentous decrease in efficiency.

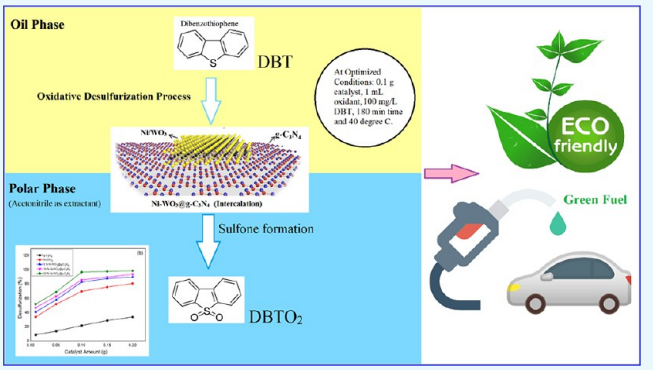

INTRODUCTION

Globally, researchers are focusing on the production of green fuels because of the environmental protection and increasing strict legislations regarding the limit of sulfur in hydrocarbons not to be more than 10 mg/L.[1−4] The major challenge is the removal of sulfur compounds such as thiophenes (Th), benzothiophene (BT), dibenzothiophene (DBT), and their derivatives due to stringent regulations in oil refineries. As we all know, the traditional desulfurization technology (hydrodesulfurization (HDS)) requires hydrogen under severe operating conditions (high temperatures and pressures) as well as it is unable to remove aromatic sulfur compounds such as DBT.[5,6] Considering the above-mentioned reasons, alternative technologies are under development, and they are adsorption,[7,8] bio-desulfurization (BD),[9] extractive desulfurization (ExD),[10] and oxidative desulfurization (ODS).[11] Among them, oxidative desulfurization could be a viable process for the removal of sulfur species from fuel oil owing to its high efficiency, economic aspect, eco-friendliness, low energy cost, handiness, and resistance to harsh operating conditions. In light of these striking properties, researchers are paying prime importance to this technique (ODS), which is a great challenge to produce green fuels.[12,13] In this technology, sulfur compounds oxidized into sulfoxides and sulfones are considered under a catalytic oxidation reaction with an oxidant such as H_2O_2.

Desulfurization assisted by an oxidative desulfurization (ODS) process is a prospective methodology for eliminating sulfur-based aromatic compounds from liquid fuels (gasoline, diesel, light diesel oil, and kerosene). During the past few decades, oxidative catalysis has enlarged substantial research interests in different applications such as water splitting, pollutant degradation, and desulfurization of fuel oil. Based on experimental evidence, above 90% of thiophene, dibenzothiophene, and their derivatives can be easily oxidized under optimized conditions.[14] Moreover, ultradeep sulfur removal by ODS can now be carried out with H_2O_2 (oxidant)-assisted

Received: February 13, 2022
Accepted: April 18, 2022
Published: April 27, 2022

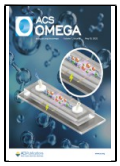

inorganic−organic hybrid catalysts when compared with traditional desulfurization methods.

Nowadays, researchers are using graphitic carbon nitride (g-C_3N_4) for the desulfurization process because of its high efficiency and some of its properties including the fact that it is composed of 2D layers of its monomer, heptazine. g-C_3N_4 belongs to that class of compounds that have a high level of nitrogen and can be synthesized by using one major type of polymerization, that is, polycondensation.[15] The monomers used for its synthesis are organic precursors, which further include cyanamide, dicyandiamide, melamine, and urea. g-C_3N_4 has its vast applications in environmental decontamination and artificial photosynthesis only because of these properties: it is abundant on earth, has a distinctive electronic configuration, and shows great physiochemical stability. The first reason behind the great chemical stability of g-C_3N_4 is the presence of carbon and nitrogen atoms that are sp^2 hybridized, and the second is the presence of a high level of nitrogen (∼55−62%).[16,17] These two described properties make g-C_3N_4 a worthy and suitable material for synthesis of hybrid materials. Additionally, transition metals such as nickel (Ni) and tungsten (W) are expected to be promising candidates to substitute precious metals (Pt, Rh, and Ir) for different catalytic activities owing to their low cost, high stability, and outstanding redox capabilities. Due to their unique physicochemical properties, nickel and tungsten are widely used in refractory alloys and as nanoparticles of metals in the form of oxides, carbides, and sulfides. Researchers are trying to develop nickel-, copper-, cobalt-, iron-, and tungsten-based catalysts supported onto thin sheets (g-C_3N_4 and graphene) for electrocatalytic (water splitting (HER and OER)) and photocatalytic applications (pollutant degradation), sensors, and many organic syntheses.[18−23]

The facts concerning oxidative desulfurization (ODS) of liquid fuels using hybrid materials are still vague. Various studies have been published on photodegradation of organic pollutants, energy production, and many other applications using hybrid materials. However, there are limited studies on the usage of a hybrid composite as a catalyst in the oxidative desulfurization (ODS) of liquid petroleum. Regarding the overhead remarks, the objective of this work was to synthesize a (Ni-WO_3@g-C_3N_4) nanocomposite and study its performance for the first time for oxidative desulfurization of model fuel (DBT) and real fuel. The prepared catalyst was characterized via Fourier transform infrared spectroscopy (FT-IR), powder X-ray diffraction (XRD), scanning electron microscopy (SEM), energy-dispersive X-ray spectroscopy (EDX), and thermogravimetric analysis (TGA) and discussed in detail. The effects of leading factors (temperature, time, DTB concentration, and the catalyst amount) on the sulfur conversion during the ODS reaction were studied in detail. As a final point, the reusability of the catalyst and applicability of the oxidation system for real fuel desulfurization are also reconnoitered.

MATERIALS AND METHODS

Materials. All the chemicals and reagents used in this study were of analytical grade; sodium tungstate dihydrate ($Na_2WO_4{\cdot}2H_2O$), melamine ($C_3H_6N_6$), and dibenzothiophene ($C_{12}H_8S$) were acquired from Sigma Aldrich Co., with hydrazine hydrate ($N_2H_4{\cdot}H_2O$) and nickel nitrate ($Ni(NO_3)_2$) from Merck. Regarding the ODS activity, model fuel (dibenzothiophene (DBT)) and real fuel (kerosene and diesel oil) were used in this study.

Methods. *Synthesis of Materials (g-C_3N_4, Ni-WO_3, and Ni-WO_3@g-C_3N_4 Composite).* The preparation of g-C_3N_4 was done via a simple decomposition method as provided in a previous study with some minor modifications.[24] Five grams of melamine was put into an aluminum crucible and heated at 550 °C in a muffle furnace (air atmosphere) for 3 h. The obtained g-C_3N_4 support material was ground via a pestle and mortar.

A solid solution of Ni-WO_3 was synthesized via hydrothermal treatment with a precursor molar ratio (1:1) as described subsequently. Typically, 5 mmol of sodium tungstate dihydrate ($Na_2WO_4{\cdot}2H_2O$) and nickel nitrate ($Ni(NO_3)_2$) was added into 100 mL of deionized water with vigorous stirring for 20 min at 30 °C. After that, 500 μL of hydrazine hydrate ($N_2H_4{\cdot}H_2O$) was added dropwise in the above solution and taken into a Teflon-assisted stainless-steel autoclave. The mixture was heated at 150 °C for 6 h and cooled down to room temperature, and the resulting product was centrifuged, washed with water (three times), and dried in an oven at 110 °C.

Different percentages of Ni-WO_3@g-C_3N_4 were prepared by varying the amount of Ni-WO_3 via a hydrothermal method. Weight percentages (20%) of the Ni-WO_3@g-C_3N_4 composite were synthesized by mixing 200 mg of prepared g-C_3N_4 with a specific amount of Ni-WO_3 in a Teflon-assisted stainless-steel autoclave and heated at 150 °C for 3 h. The prepared materials were calcined at 400 °C in a muffle furnace with a heating rate of 5 °C/min. The synthesized composite (Ni-WO_3@g-C_3N_4) was cooled down to room temperature and ground with a pestle and mortar. Moreover, we also used Ni-WO_3 and g-C_3N_4 for oxidative desulfurization activity for comparison purposes.

Oxidative Desulfurization Process (ODS). Model fuel was prepared by dissolving a specific quantity of DBT (e.g., 100 mg/L) into *n*-hexane (50 mL) as a source of sulfur; acetonitrile (30 mL as an extractant) and 0.1 g of (20% Ni-WO_3@g-C_3N_4) were added into a flask and placed in the dark for 20 min for adsorption−desorption equilibrium. Afterward, a known amount of (e.g., 1 mL of 30%) H_2O_2 was injected to the flask and stirred vigorously at a specified temperature and time (e.g., 40 °C for 60 min). The dibenzothiophene sulfone and sulfoxide formation was extracted in the acetonitrile phase that was investigated by thin-layer chromatography (TLC), the remaining concentration of DBT in the *n*-hexane phase was analyzed via a UV−vis spectrophotometer (at λ_{max} = 283 nm, $n-\pi^*$), and total sulfur was analyzed by PETRA X-ray fluorescence (ASTM D-4294, wt %) at different time intervals. Moreover, the specific gravity (ASTM D-1298 at 15.6 °C), the salt in fuel oil (ASTM D-3230 at ptb), the water content (ASTM D-4006 in wt %), and distillation (ASTM D-86 in °C) were also determined. The percentage efficiency for the removal of the sulfur content from both model and real fuel oil was determined via the given equation (eq 1)

$$\text{sulfur removal efficiency (\%)} = \frac{S_i - S_f}{S_i} \times 100 \quad (1)$$

Instrumentation. XRD patterns of g-C_3N_4, Ni-WO_3, and the 20% synthesized composite Ni-WO_3@g-C_3N_4 were analyzed via powder X-ray diffraction by using Cu Kα of 1.54 Å in the 2θ range of 3−70° with a 2° per min scan rate.

https://doi.org/10.1021/acsomega.2c00886
ACS Omega 2022, 7, 15809−15820

For the vibrational band study, FT-IR spectra of prepared materials were collected by an IR-TRACER-100 (4000−400 cm^{-1}), with the surface morphology via scanning electron microscopy (SEM) (NOVA NANO) and elemental analysis via energy-dispersive X-ray spectroscopy (EDX). Moreover, the mass loss (wt %) was also evaluated via thermogravimetric analysis (TGA) in an inert atmosphere in the range of 40−800 °C. To quantify the sulfur components in both model and real fuel, samples were analyzed via PETRA X-ray fluorescence (PETRA-XRF, ppm, ASTM D-4294). Additionally, other fuel properties (water content, specific gravity, salt in fuel, and distillation) were determined via a water content tester (China PT-D4006-8929A, vol %, ASTM D-4006), a hydrometer (g/mL at 15.6 °C, ASTM D-1298), and a distillation tester (PMD 110, PAC, ASTM D-86).

RESULTS AND DISCUSSION

FT-IR. FT-IR studies were carried out to investigate the functional groups present in synthesized g-C_3N_4 and the Ni-

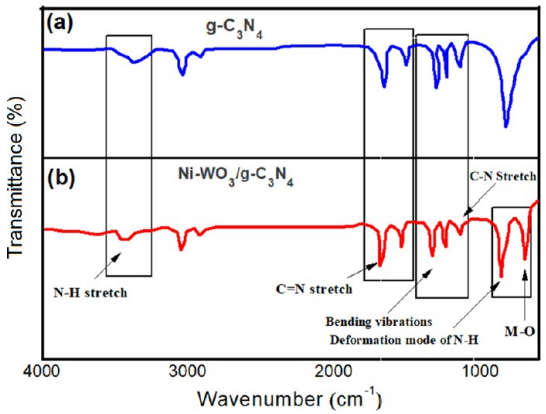

Figure 1. IR vibrational analysis of graphitic carbon nitride (g-C_3N_4) (a) and nanocomposite Ni-WO_3@g-C_3N_4 (b).

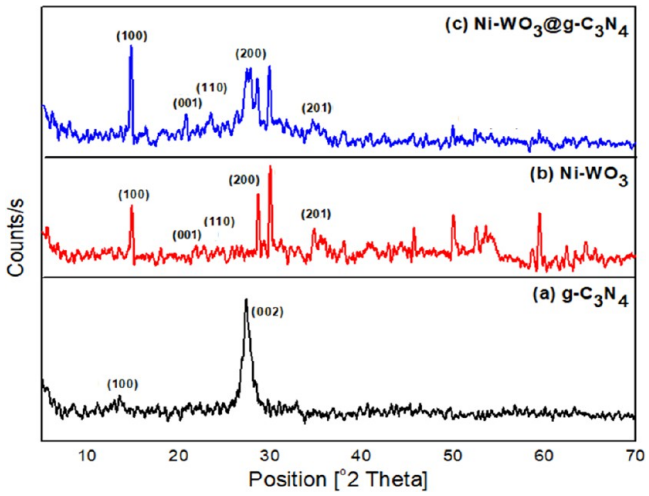

Figure 2. XRD spectra of (a) g-C_3N_4, (b) Ni-WO_3, and (c) Ni-WO_3@g-C_3N_4.

WO_3@g-C_3N_4 composite in the range of 4000−400 cm^{-1} as shown in Figure 1. The observed vibrational bands at 1630 and 1230 cm^{-1} indicate the presence of C═N and C−N stretching in g-C_3N_4, respectively. The characteristic bands observed in the range of 3500−3200 and 1575 cm^{-1} correspond to N−H stretching and the bending vibrations in g-C_3N_4, respectively. The other peaks observed at 860, 1320, and 1409 cm^{-1} are due to the deformation mode of N−H and the bending vibration as reported previously.[25,26] All the peaks remain identical in both (g-C_3N_4 and the Ni-WO_3@g-C_3N_4 composite) except one peak that is observed only in the Ni-WO_3@g-C_3N_4 composite in the range of 600−450 cm^{-1} owing to the M−O peak. All the observed characteristic vibrational bands give confirmation of the successful synthesis of g-C_3N_4 and Ni-WO_3@g-C_3N_4.

XRD Pattern. XRD patterns of g-C3N_4, Ni-WO_3, and the synthesized composite Ni-WO_3@g-C_3N_4 were analyzed via powder X-ray diffraction by using Cu Kα of 0.154 nm, in the 2θ range of 3−70° with a 2° per min scan rate. In the XRD spectra of g-C_3N_4 (Figure 2a), there are two characteristic peaks that appeared at 2θ = 13.43 and 27.40° corresponding to the basal planes of (100) and (002), respectively, as matched with JCPDS card no. 01-087-1526 as well as in good agreement with a reported study.[27] The basal plane (002) is attributed to the interlayer stacking of conjugated aromatic systems in g-C_3N_4, which corresponds to the flake-like structure with a *d*-spacing of 0.33 nm, and the (001) plane is due to ordering of tri-*s*-triazine units. In the XRD pattern of Ni-WO_3 (Figure 2b), the characteristic peak positions with the crystal planes are as follows: 2θ = 14.19 (100), 22.78 (001), 24.78 (110), 29.13 (200), and 36.5° (201) are in good agreement with JCPDS card no. 033-1387 due to the phase of WO_3.[28] Similarly, the XRD pattern of Ni-WO_3@g-C_3N_4 (Figure 2c) exhibits 2θ = 14.21 (100), 22.77 (001), 24.65 (110), 29.23 (200), and 36.61° (201). Both (g-C_3N_4 and Ni-WO_3) peaks are observed in the spectra of Ni-WO_3@g-C_3N_4, which revealed that the Ni-WO_3@g-C_3N_4 composite was synthesized successfully.[29] The XRD patterns of both pristine Ni-WO_3 and Ni-WO_3@g-C_3N_4 samples indicate no peaks of the new phase that can be detected. However, the intensity of planes becomes lower in the Ni-WO_3@g-C_3N_4 composite pattern due to the presence of Ni -WO_3. The average crystallite size was calculated via the Scherrer equation (eq 2):

$$D = \frac{k\lambda}{\beta \cos\theta} \quad (2)$$

where D is the average crystallite size, k is the Scherrer constant (0.9), λ equals 0.154 nm, β is the full width at half-maximum (FWHM), and θ is the angle of reflection. The calculated average crystallite sizes of g-C_3N_4, Ni-WO_3, and Ni-WO_3@g-C_3N_4 are 14.2, 55, and 50.4 nm, respectively.

SEM and EDX. The surface morphology of g-C_3N_4 and Ni-WO_3@g-C_3N_4 was analyzed via a NOVA NANO SEM. It is evident from the SEM image in Figure 3,ba that the surface of the g-C_3N_4 material is noticed to be a wrinkled sheet and solid agglomerates, which formed a stacked structure. It can be seen that Ni-WO_3 particles are well-decorated on the g-C_3N_4 surface with an interesting morphology (Figure 3c−f). The Ni-WO_3 particles appeared on the surface with a proper geometry (spherical particles) rather than wrinkled sheets. Figure 4,ba shows the elemental analysis of g-C_3N_4 and the Ni-WO_3@g-C_3N_4 composite collected from energy-dispersive X-ray spectroscopy (EDX). Figure 4b indicates the presence of Ni and W loaded onto g-C_3N_4 as absent in the EDX spectra of simple g-C_3N_4. The elemental composition in g-C_3N_4 is 34.85 wt % C and 65.15 wt % N and in Ni-WO_3@g-C_3N_4 is 37.34 wt % C, 30.79 wt % N, 13.28 wt % O, 4.93 wt % Ni, and 13.66 wt % W. The elemental mappings of C, O, N, Ni, and W in Ni-WO_3@g-C_3N_4 are shown in light green, red, dark green,

https://doi.org/10.1021/acsomega.2c00886
ACS Omega 2022, 7, 15809−15820

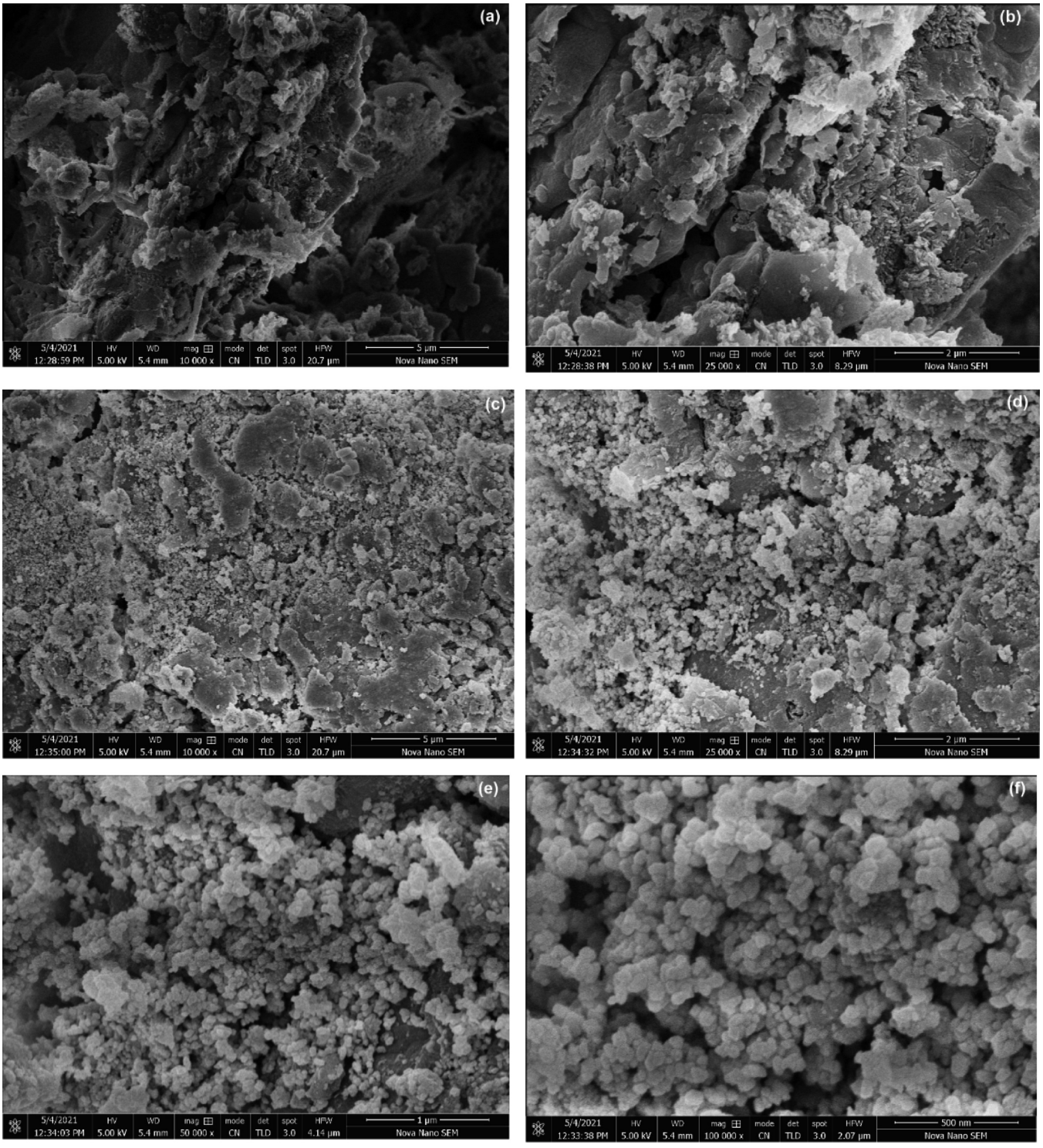

Figure 3. SEM micrographs of g-C_3N_4 (a,b) and Ni-WO_3@g-C_3N_4 (c–f).

purple, and yellow colors, respectively. These EDX peaks confirm the loading of Ni-WO_3 onto g-C_3N_4 as the morphology is also different after loading.

Thermogravimetric Analysis (TGA). To quantify the mass loss (%), the prepared materials have been examined by TGA (at 40–800 °C) under an inert atmosphere. It can be seen from Figure 5 that there is a slight decrease in weight loss (%) in g-C_3N_4 below 200 °C (18%) due to volatilization of adsorbed water or other impurities. The significant weight loss observed after 600 °C (72%) corresponds to the lower thermal stability of g-C_3N_4 as compared to the nanocomposite. In the Ni-WO_3@g-C_3N_4 composite curve, a 5% mass loss occurred below 200 °C due to dehydration of water. Condensation of melamine and release of ammonia gas lead to a 9% loss after 400 °C in the nanocomposite. Pure g-C_3N_4 has a larger weight loss than the composite in the range of 500–700 °C that revealed that the nanocomposite is more efficient for catalytic activity owing to thermal stability.[30]

Optimization of DBT Removal from Model Fuel Oil. In order to check the catalytic activity of the prepared catalyst

https://doi.org/10.1021/acsomega.2c00886
ACS Omega 2022, 7, 15809–15820

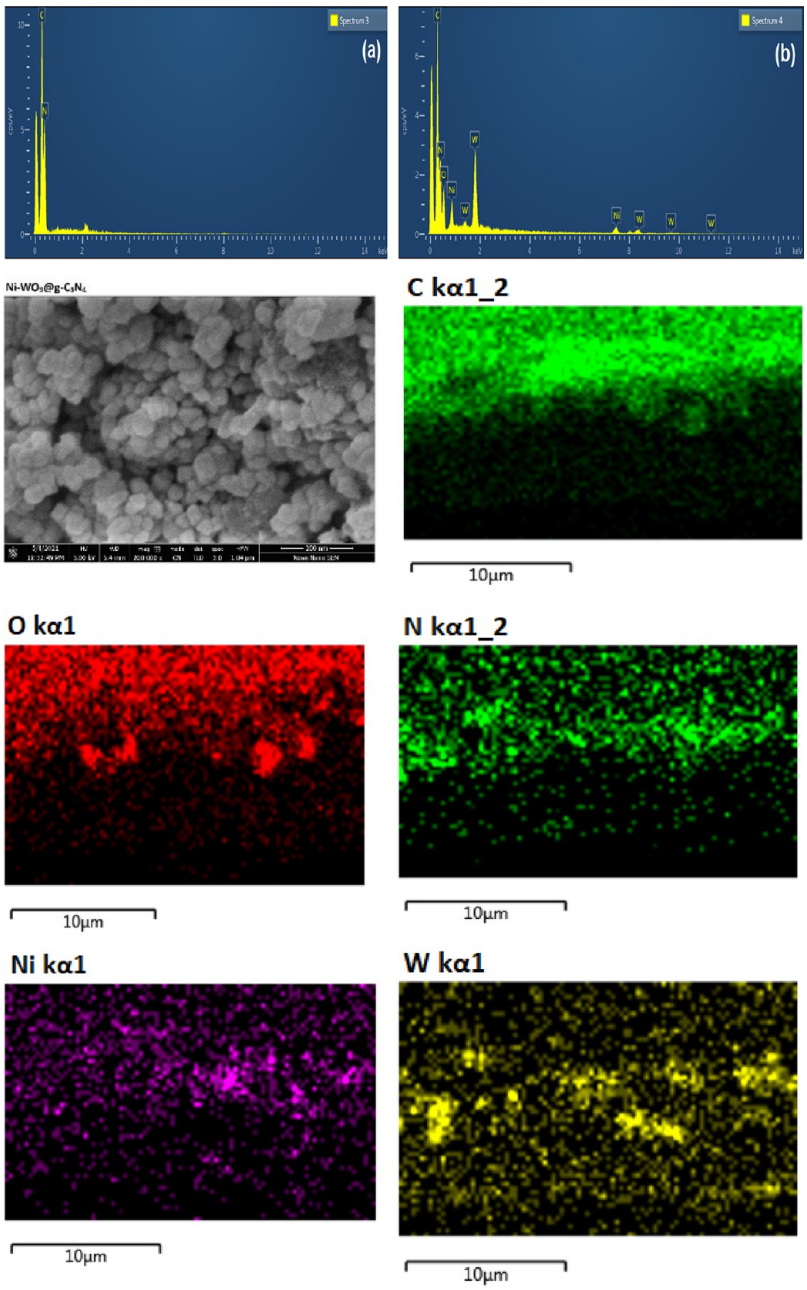

Figure 4. EDX of g-C_3N_4 (a) and Ni-WO_3@g-C_3N_4 composite (b) and EDX mapping of C, O, N, Ni, and W in the composite.

(20% Ni-WO_3@g-C_3N_4), multiple parameters have been optimized. Temperature also played a crucial role in the oxidative desulfurization system. The effect of time and temperature on DBT removal (%) is shown in Figure 6a at different times (30−180 min) and temperatures (25−40 °C) by taking 0.1 g of the synthesized catalyst, 1 mL of an oxidant, 50 mL of DBT solution (100 mg/L), and 30 mL of acetonitrile as an extractant. More than 90% DBT removal was achieved using 180 min of time. It was assumed that DBT removal might be kinetically limited at low temperatures and increased with an increase in the temperature until 40 °C.[31] Beyond 40 °C, no significant change has been observed, which might be due to decomposition of H_2O_2 at high temperatures. The maximum efficiency (97%) was attained at 40 °C in 180 min, and this time was optimized for further studies.

The effect of different catalysts (bare g-C_3N_4, Ni-WO_3, and Ni-WO_3@g-C_3N_4) were investigated keeping other parameters constant (0.1 g of the catalyst, 50 mL of DBT solution (100 mg/L in *n*-hexane), 1 mL of oxidant (H_2O_2), a time duration of 180 min, and a temperature of 40 °C). It can be seen that g-C_3N_4 shows an about 30% removal efficiency, which might be closely related to the adsorption phenomenon to some extent. Ni-WO_3 and 5, 10, and 20% Ni-WO_3@g-C_3N_4 activities for DBT removal were compared in which Ni-WO_3 supported onto g-C_3N_4 showed better results than Ni-WO_3. Overall, 20% Ni-WO_3 loaded onto g-C_3N_4 shows the maximum desulfurization efficiency as shown in Figure 6b providing maximum active sites for ODS. Additionally, the catalyst amount has direct relation with DBT removal (%).[32]

The effect of DBT concentration on desulfurization of fuel oil was monitored by varying the DBT concentration (50, 100,

https://doi.org/10.1021/acsomega.2c00886
ACS Omega 2022, 7, 15809−15820

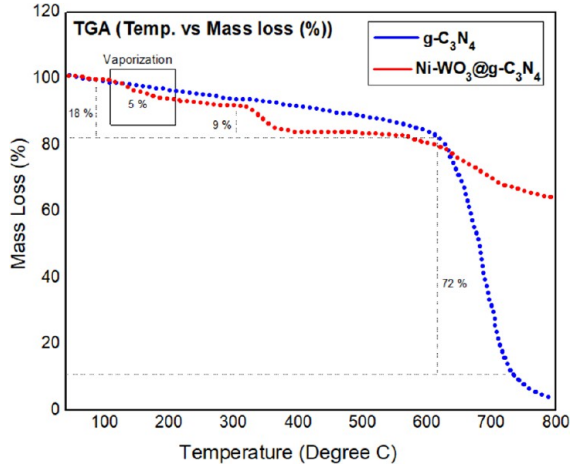

Figure 5. TGA mass loss curves of g-C_3N_4 and Ni-WO_3@g-C_3N_4.

200, and 400 mg/L) with other parameters kept constant (0.1 g of the catalyst, a volume of 50 mL, 1 mL of the oxidant (H_2O_2), a time duration of 180 min, and a temperature of 40 °C). Figure 6c shows that as we increased the DBT concentration from 50 to 400 mg/L, the removal efficiency decreased. The removal efficiency is affected, as it limits the available catalytic site of Ni-WO_3@g-C_3N_4 at a high DBT concentration, but it is still able to work with a lower efficiency.[32] When a lower concentration of DBT is present, the DBT removal is faster as a higher number of sites are present. It was concluded that the greater is the presence of catalytic sites, the lower is the concentration of DBT molecules and the more effective will be the desulfurization done at optimized conditions.

The effect of H_2O_2 as an oxidant on desulfurization has been investigated by varying the amount of the oxidant (0.5, 1, 2, and 3 mL) keeping other parameters constant. It was observed that >90% DBT removal can be achieved by using 1 mL of H_2O_2 as an oxidant as shown in Figure 6d. Moreover, no significant increase in desulfurization has been observed by increasing the H_2O_2 amount. Hence, 0.1 g of the catalyst (Ni-WO_3@g-C_3N_4) can be effectively used to remove (>97%) 100 mg/L DBT at 40 °C within 180 min.

Kinetics, Thermodynamics, and Mechanism of Oxidative Desulfurization via Ni-WO_3@g-C_3N_4. The kinetic study of DBT removal via the ODS process was examined by applying a pseudo first-order kinetic model.[31,32] The plot of C_F/C_i vs time (min) at different temperatures is shown in Figure 7a, and the regression coefficients (R^2) were found to be in the range of 0.75−0.85, where C_i and C_F are the initial and final concentrations of DBT. The results depict that DBT removal by using Ni-WO_3@g-C_3N_4 followed a pseudo first-order kinetic model with rate constants (k, min^{-1}) of 0.0074, 0.0078, 0.0082, and 0.0082 at 25, 30, 35, and 40 °C, respectively. Additionally, the activation energy (E_a) of the ODS process was calculated via the Arrhenius plot ($1/T$ vs ln k, Figure 7b) as previously reported, and the E_a for the current study is 6.14 kJ/mol.

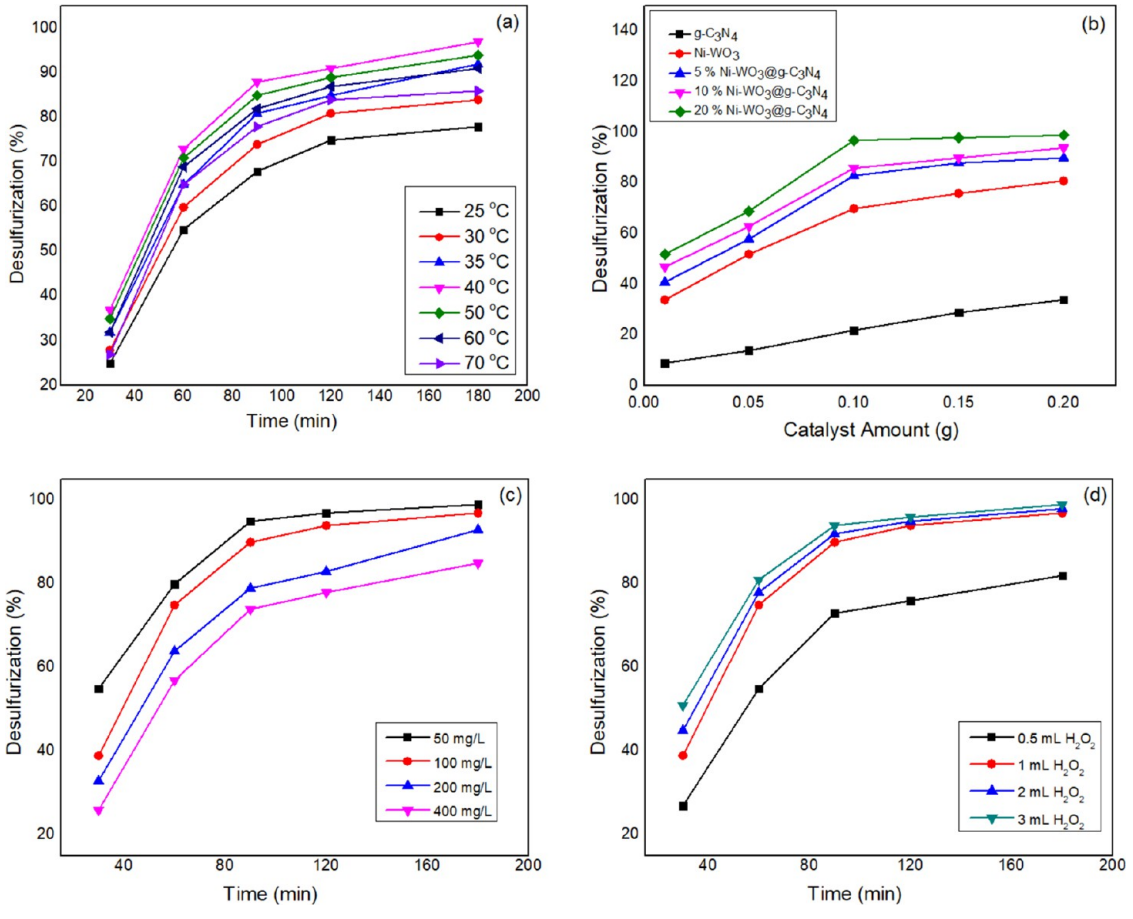

Figure 6. Effect of the temperature (a), catalyst amount (b), DBT concentration (c), and amount of H_2O_2 (d) on desulfurization.

https://doi.org/10.1021/acsomega.2c00886
ACS Omega 2022, 7, 15809−15820

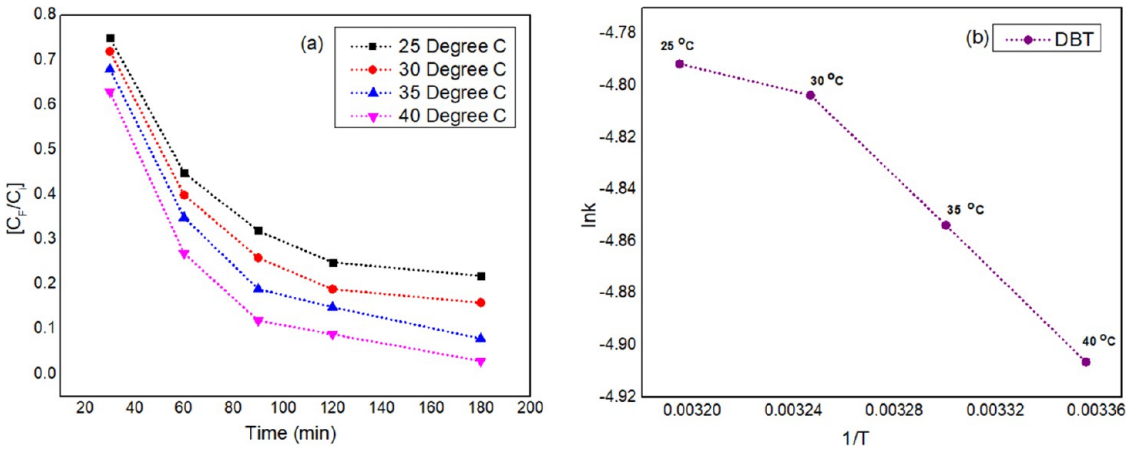

Figure 7. Plot of C_F/C_i vs time (min) for DBT removal via the ODS process (a) and $1/T$ vs ln k (b).

Table 1. Thermodynamic Parameters for DBT Removal via ODS

	ΔG (kJ mol^{-1})					
catalytic system	298.5 K	303.5 K	308.5 K	313.5 K	ΔH (kJ mol^{-1})	ΔS (kJ mol^{-1} K^{-1})
Ni-WO_3@g-C_3N_4/H_2O_2	−0.014	−0.024	−0.044	−0.071	354	0.004

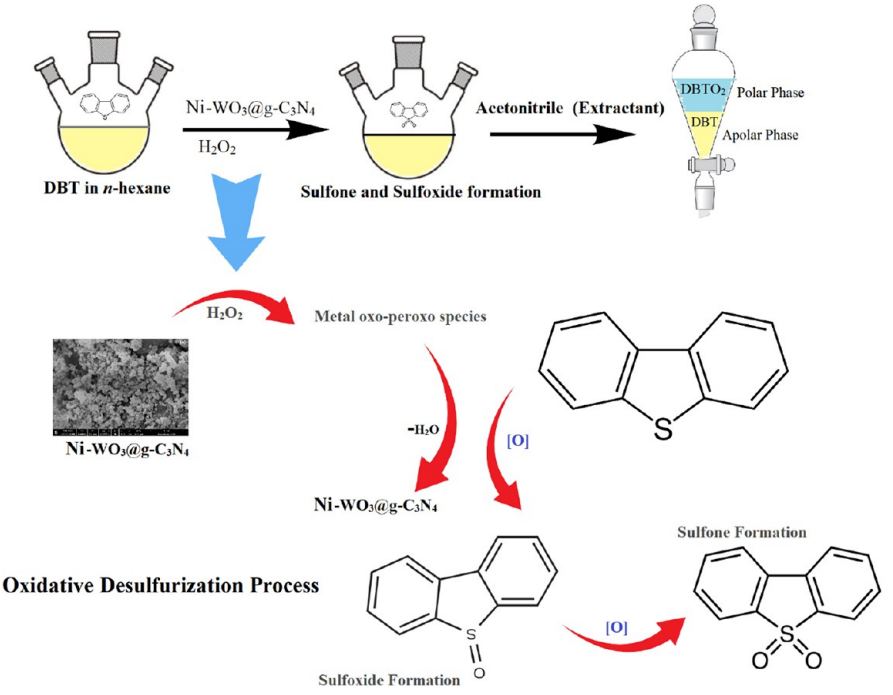

Figure 8. Possible mechanism of ODS for DBT.

To understand the temperature effect on DBT oxidation, standard Gibbs free energy (ΔG),standard entropy (ΔS), and standard enthalpy ($\Delta H°$) were determined by using the Eyring equation[33,34] as given below:

$$\ln K_c = -\frac{\Delta H}{RT} + \frac{\Delta S}{R} \quad (3)$$

where K_c is the equilibrium constant and T is the temperature in Kelvin. The standard Gibbs free energy was calculated using the following equation:[35]

$$\Delta G = -RT \ln K_c \quad (4)$$

The obtained results showed that positive ΔH and positive ΔS from the plot of $1/T$ vs ln K_c correspond to the endothermic process and randomness in reaction media, respectively, as given in Table 1. The negative value of ΔG revealed that DBT removal via Ni-WO_3@g-C_3N_4 is a spontaneous and thermodynamically feasible ODS process, and a more negative value has been observed at 313 K.

Overall, the remarkable activity of the catalyst for DBT removal is the result of morphological effects such as the crystallite size and the surface area. Based on experimental evidence and the optimization study, the proposed mechanism for ODS of DBT-based model fuel is shown in Figure 8. It is a three-step mechanism as follows: (a) formation of metal oxo-

https://doi.org/10.1021/acsomega.2c00886
ACS Omega 2022, 7, 15809−15820

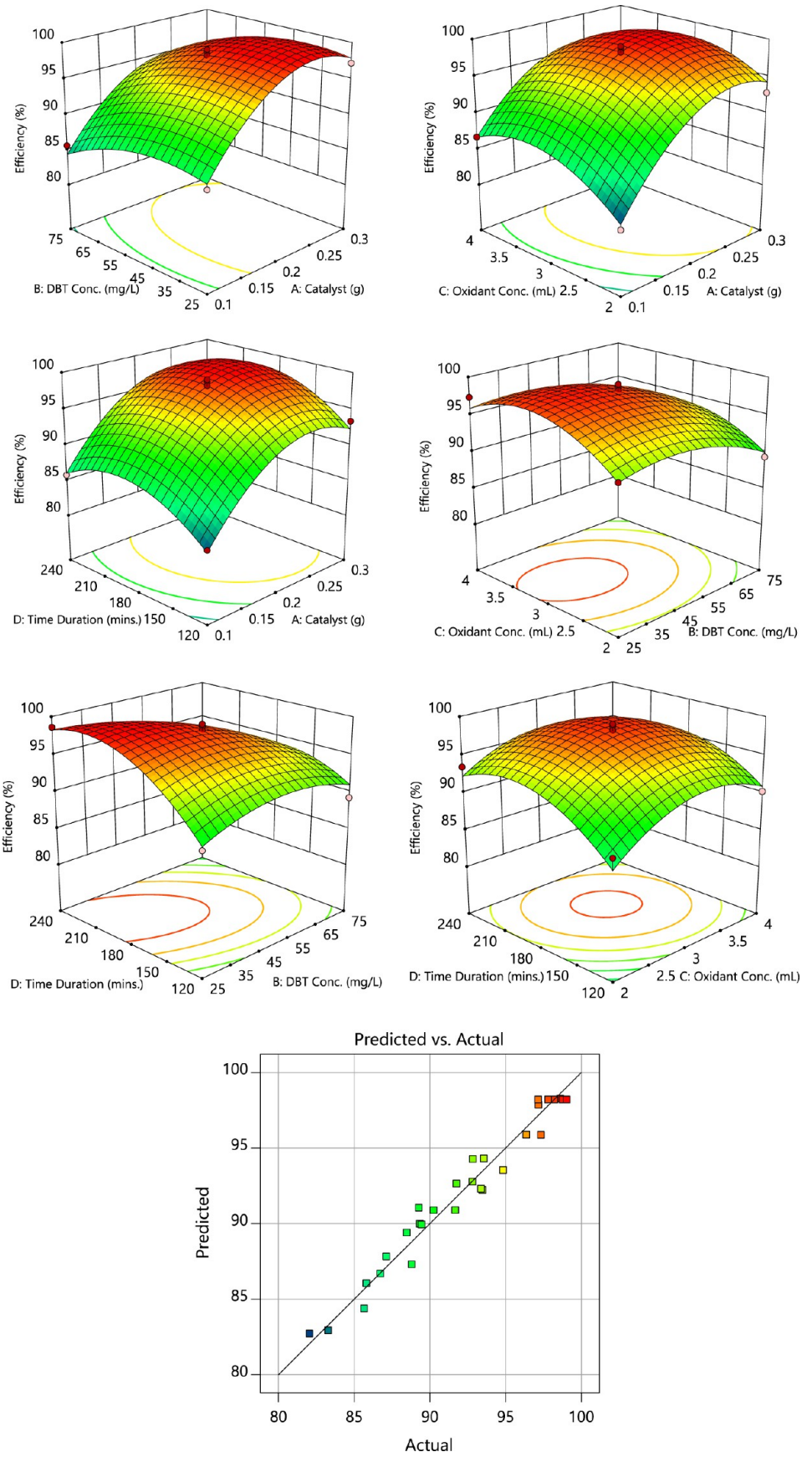

Figure 9. RSM 3D graphs presenting the effect of various factors on desulfurization of fuel oil.

https://doi.org/10.1021/acsomega.2c00886
ACS Omega 2022, 7, 15809−15820

Table 2. Analysis of ANOVA from Obtained Results

source	sum of squares	Df	mean	*F*-value	*p*-value	comments
model	656.9119	14	46.92228064	27.6046	9.09×10^{-8}	significant
A-catalyst	275.8084	1	275.8084083	162.2594	4.33×10^{-9}	
B-DBT conc.	45.04688	1	45.046875	26.50129	0.000148	
C-oxidant conc.	12.04003	1	12.04003333	7.083209	0.018609	
D-time duration	33.60053	1	33.60053333	19.76735	0.000554	
AB	0.1936	1	0.1936	0.113896	0.740758	
AC	3.8809	1	3.8809	2.283152	0.153025	
AD	0.055225	1	0.055225	0.032489	0.859541	
BC	1.199025	1	1.199025	0.705392	0.415091	
BD	24.8004	1	24.8004	14.59019	0.001876	
CD	2.512225	1	2.512225	1.477954	0.244198	
$A\hat{A}^2$	167.7335	1	167.7335353	98.67844	1.01×10^{-7}	
$B\hat{A}^2$	31.75715	1	31.75714883	18.68288	0.000702	
$C\hat{A}^2$	84.5989	1	84.5988995	49.76994	5.73×10^{-6}	
$D\hat{A}^2$	94.8476	1	94.84760221	55.7993	3.01×10^{-6}	
residual	23.79719	14	1.699799167			
lack of fit	21.55111	10	2.155110833	3.837995	0.103388	not significant
pure error	2.24608	4	0.56152			
cor total	680.7091	28				
std. dev.	1.303763		$R\hat{A}^2$	0.965041		
mean	92.10552		adjusted $R\hat{A}^2$	0.930081		
C.V. %	1.415511		predicted $R\hat{A}^2$	0.812484		
			acceptable precision	16.57495		

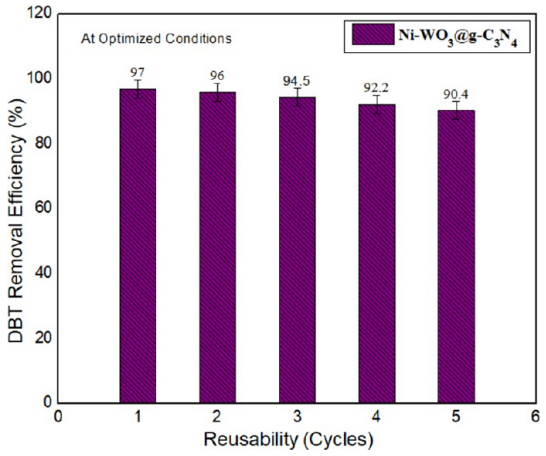

Figure 10. Desulfurization efficiency of Ni-WO_3@g-C_3N_4 in multiple cycles.

Table 3. ODS of Kerosene and Diesel Oil via Ni-WO_3@g-C_3N_4

		diesel oil		kerosene oil	
tests	method no.	before ODS	after ODS	before ODS	after ODS
specific gravity (g/mL at 15.6 °C)	ASTM D-1298	0.879	0.875	0.833	0.831
total sulfur by PETRA X-ray fluorescence (ppm)	ASTM D-4294	4630	474	1635	143
water content by distillation (vol %)	ASTM D-4006	nil	nil	nil	nil
distillation (°C)					
50%	ASTM D-86	285	281	237	236
90%		345	343	303	301

peroxo species by attack of H_2O_2 nucleophiles, (b) loss of water molecules, and (c) formation of first sulfoxides and then sulfones. In the presence of a graphitic carbon nitride-based nanocomposite and hydrogen peroxide, a simple chemical process implied that oxygen radicals from hydrogen peroxide attack the electron-rich sulfur atom of DBT molecules resulting in the formation of sulfoxides and then sulfones. Additionally, the metal oxo-peroxo species are generated by the reaction of an oxidizing agent with the catalyst. The nucleophilic attack of peroxo species on sulfur changed it into sulfoxides and corresponding sulfones.[36,37]

Desulfurization Optimization through the Response Surface Methodology (RSM). For the purpose of theoretical optimization, the RSM was used for optimizing the optimum reaction parameters and mathematically predicting the efficiency of desulfurization of fuel oil. The four input variables include the (a) catalyst concentration (in g), (b) DBT concentration (in mg/L), (c) oxidant concentration (in mL), and (d) time duration (in min), and the efficiency of desulfurization was taken as an output variable. The Box–Behnken design (BBD) technique was followed for the optimization purpose, and in total, 29 experimental runs were carried out for varied combinations of input variables.

$$\begin{aligned}\text{efficiency} = {} & 98.202 + 4.79417A + -1.9375B + 1.00167C \\ & + 1.67333D + -0.22AB - 0.985AC \\ & + 0.1175AD - 0.5475BC - 2.49BD \\ & - 0.7925CD - 5.08517A^2 - 2.21267B^2 \\ & - 3.61142C^2 - 3.82392D^2\end{aligned}$$

The above equation is the coded equation of the prediction model for calculating the efficiency of desulfurization. From the equation, it can be inferred that the catalyst concentration, oxidant concentration, and time duration had a positive effect, while the DBT concentration had a negative effect on the overall efficiency. From surface plots, it can be noted that efficiency increased with an increase in the catalyst

https://doi.org/10.1021/acsomega.2c00886
ACS Omega 2022, 7, 15809−15820

Table 4. Comparison with Previously Reported Studies (g-C_3N_4-Based Catalysts)

material	sulfur species	oxidant	DBT concentration (mg/L)	efficiency (%)	ref.
g-C_3N_4	DBT	TBHP	500	<10	38
MoO_2/g-C_3N_4			500	100	
Fe-CN-NHχ	H_2S		5000	∼100	15
WO_3/g-C_3N_4	DBT	H_2O_2	500	91.2	39
P-doped g-C_3N_4 nanosheet-supported V-based nanocomposites (V/P-CN)	DBT	TBHP	500	∼100	40
C_{14}PPMo/g-C_3N_4	DBT	H_2O_2	500	∼100	41
	4,6-DMDBT		250	94.8	
X-MoO_2/g-C_3N_4	DBT	H_2O_2	500	96	42
NiW/rGO	DBT	H_2O_2	500	>90	43
CoW/rGO			500	∼100	
CoO/g-C_3N_4	DBT	H_2O_2		86.7	44
Ni-WO_3@g-C_3N_4	DBT	H_2O_2	100	97	present study
	diesel		4630	89.5	
	kerosene		1635	91.5	

concentration, oxidant concentration, and time duration (explain this phenomenon). On the other hand, the efficiency decreased with an increase in DBT concentration (Figure 9). The maximum efficacy achieved 99% for the optimum parameters. From ANOVA (Table 2), it can be noted that the prediction model is highly significant with its lack of fit being not significant, thereby confirming the model to be highly reliable. Supporting this, the R^2 of the model was calculated to be 0.965 and its adjusted R^2 to be 0.9301, which signifies that the accuracy of the developed model will be nearly 97%. In other words, the average standard deviation between the experimental and predicted values will be around 1.3%. Figure 9 (predicted vs actual) illustrates the plot between the experimental and theoretical values of the developed model.

Reusability of the Catalyst. We have also tested the prepared materials for reusability and regeneration processes under similar conditions (0.1 g of the catalyst, 50 mL of 100 mg/L DBT solution, 30 mL of an extractant, 1 mL of an oxidant, and 180 min at 40 °C). At the end of each oxidation reaction, the catalyst was separated by a simple filtration method, washed with dichloromethane (CH_2Cl_2), and dried in an oven at 90 °C. The obtained findings revealed that no significant decrease in efficiency has been observed after two cycles (only 1%) and it decreased to some extent (about 5−6%) after further three cycles as shown in Figure 10. It means that the prepared material shows promising reusability and high stability. The catalytic activity might be decreased after many cycles due to a decrease in active sites as well as the mass loss of the catalyst.

Oxidative Desulfurization (ODS) of Real Fuel Oil. The oxidative desulfurization (ODS) of commercially accessible fuel samples (diesel and kerosene) was also done by using the Ni-WO_3@g-C_3N_4 nanocomposite and H_2O_2 as an oxidant under optimized conditions (0.2 g of the catalyst, 3 mL of an oxidant, 50 mL of the fuel sample, and a time duration of 180 min at 40 °C). PETRA X-ray fluorescence (XRF total sulfur analyzer, ASTM D-4294 in ppm) was employed to quantify the amount of sulfur before and after ODS, and the total sulfur contents in diesel oil and kerosene were 4630 and 1635 ppm, respectively. Additionally, other fuel properties were also examined such as the water content (ASTM D-4006), specific gravity (ASTM D-1298), and distillation (ASTM D-86) as given in Table 3. The obtained findings revealed that 89.5 and 91.2% sulfur elimination was achieved for diesel and kerosene, respectively, and other fuel properties are almost similar. Moreover, pure g-C_3N_4 was also used for the same purpose as it also shows efficiency to some extent, which might be due to the adsorption phenomenon, as well as oxidative properties and is not comparable with the composite.

Comparison with Other Reported Methods. Considering inorganic−organic hybrid materials, limited studies are available for DBT removal through the oxidative desulfurization route. We cannot make comparison effectively for ODS of DBT and real fuel oil, but some of the available studies have been compared and are given in Table 4.

CONCLUSIONS

A highly efficient and eco-friendly material has been synthesized and used for the first time for oxidative desulfurization of DBT model fuel as well as real fuel (diesel and kerosene oil). XRD results depict that the average crystallite size of Ni-WO_3@g-C_3N_4 is 50.36 nm and it has a monoclinic phase. The SEM morphology of prepared materials indicates that spherical particles are well-decorated on the surface of g-C_3N_4. The prepared materials showed outstanding performance for DBT removal from model fuel with 97% and real fuel (diesel with 89.5% and kerosene with 91.5%) via ODS. Multiple factors have been applied to optimize the process in which the time, the catalyst amount, and the oxidant amount have direct relation and DBT concentration has indirect relation with removal efficiency. This ODS process followed pseudo first-order kinetics, and a negative value of ΔG showed the spontaneity in the reaction system. Moreover, response surface methodology (RSM) 3D plots based on the Box−Behnken design were used to optimize the desulfurization of fuel oil. The nanocomposite showed promising reusability up to five times with no significant change in desulfurization efficiency. Thus, the entire study confirms the prominence of the prepared nanocomposite for efficient production of sulfur-free oil.

AUTHOR INFORMATION

Corresponding Author

Amir Waseem − *Department of Chemistry, Quaid-i-Azam University, Islamabad 45320, Pakistan;* orcid.org/0000-0001-8414-0374; Email: amir@qau.edu.pk

https://doi.org/10.1021/acsomega.2c00886
ACS Omega 2022, 7, 15809−15820

Authors

Muhammad Saeed − *School of Chemistry, University of the Punjab, Lahore 54590, Pakistan*

Mamoona Munir − *Department of Biological Sciences, International Islamic University, Islamabad 44000, Pakistan*

Azeem Intisar − *School of Chemistry, University of the Punjab, Lahore 54590, Pakistan*

Complete contact information is available at: https://pubs.acs.org/10.1021/acsomega.2c00886

Notes

The authors declare no competing financial interest.

■ ACKNOWLEDGMENTS

The authors are grateful to the Pakistan Science Foundation for financial assistance under project no. PSF-NSFC-IV/Chem/C-QAU (27).

■ REFERENCES

(1) Saeed, M.; Howari, H.; Alhodaib, A.; Waseem, A. Synthesis, Characterization and Application of Organoclay for Adsorptive Desulfurization: Isothermal; Kinetic and Thermodynamics Studies. *Sci. Rep.* **2021**, DOI: 10.21203/rs.3.rs-1208540/v1.

(2) Wu, J.; Li, J.; Liu, J.; Bai, J.; Yang, L. A Novel Nb 2 O 5 /Bi 2 WO 6 Heterojunction Photocatalytic Oxidative Desulfurization Catalyst with High Visible Light-Induced Photocatalytic Activity. *RSC Adv.* **2017**, *7*, 51046−51054.

(3) Jiang, Z.; Lü, H.; Zhang, Y.; Li, C. Oxidative Desulfurization of Fuel Oils. *Chin. J. Catal.* **2011**, *32*, 707−715.

(4) Ismagilov, Z.; Yashnik, S.; Kerzhentsev, M.; Parmon, V.; Bourane, A.; Al-Shahrani, F. M.; Hajji, A. A.; Koseoglu, O. R. Oxidative Desulfurization of Hydrocarbon Fuels. *Catal. Rev.* **2011**, *53*, 199−255.

(5) Yue, D.; Lei, J.; Zhou, L.; Du, X.; Guo, Z.; Li, J. Oxidative Desulfurization of Fuels at Room Temperature Using Ordered Meso/Macroporous H3PW12O40/SiO2 Catalyst with High Specific Surface Areas. *Arab. J. Chem.* **2020**, *13*, 2649−2658.

(6) Cui, J.; Wang, G.; Liu, W.; Ke, P.; Tian, Q.; Li, X.; Tian, Y. Synthesis BiVO4 Modified by CuO Supported onto Bentonite for Molecular Oxygen Photocatalytic Oxidative Desulfurization of Fuel under Visible Light. *Fuel* **2021**, *290*, 120066.

(7) Rekos, K.; Kampouraki, Z. C.; Panou, C.; Baspanelou, A.; Triantafyllidis, K.; Deliyanni, E. Adsorption of DBT and 4,6-DMDBTon Nanoporous Activated Carbons: The Role of Surface Chemistry and the Solvent. *Environ. Sci. Pollut. Res.* **2021**, *28*, 59050−59062.

(8) Wahab, N.; Saeed, M.; Ibrahim, M.; Munir, A.; Saleem, M.; Zahra, M.; Waseem, A. Synthesis, Characterization, and Applications of Silk/Bentonite Clay Composite for Heavy Metal Removal From Aqueous Solution. *Front. Chem.* **2019**, *7*, 654.

(9) Stylianou, M.; Vyrides, I.; Agapiou, A. Oil Biodesulfurization: A Review of Applied Analytical Techniques. *J. Chromatogr., B* **2021**, *1171*, 122602.

(10) Jin, N.; Yue, J.; Zhao, Y.; Lü, H.; Wang, C. Experimental Study and Mass Transfer Modelling for Extractive Desulfurization of Diesel with Ionic Liquid in Microreactors. *Chem. Eng. J.* **2021**, *413*, 127419.

(11) Chen, L.; Yuan, Z. Y. Design Strategies of Supported Metal-Based Catalysts for Efficient Oxidative Desulfurization of Fuel. *J. Ind. Eng. Chem.* **2022**, *108*, 1−14.

(12) Nie, Y.; Dong, Y.; Bai, L.; Dong, H.; Zhang, X. Fast Oxidative Desulfurization of Fuel Oil Using Dialkylpyridinium Tetrachloroferrates Ionic Liquids. *Fuel* **2013**, *103*, 997−1002.

(13) Shafiq, I.; Shafique, S.; Akhter, P.; Ishaq, M.; Yang, W.; Hussain, M. Recent Breakthroughs in Deep Aerobic Oxidative Desulfurization of Petroleum Refinery Products. *J. Cleaner Prod.* **2021**, *294*, 125731.

(14) Ahmadian, M.; Anbia, M. Oxidative Desulfurization of Liquid Fuels Using Polyoxometalate-Based Catalysts: A Review. *Energy Fuels* **2021**, *35*, 10347−10373.

(15) Lei, G.; Zhao, W.; Shen, L.; Liang, S.; Au, C.; Jiang, L. Isolated Iron Sites Embedded in Graphitic Carbon Nitride (g-C3N4) for Efficient Oxidative Desulfurization. *Appl. Catal. B Environ.* **2020**, *267*, 118663.

(16) Lei, G.; Cao, Y.; Zhao, W.; Dai, Z.; Shen, L.; Xiao, Y.; Jiang, L. Exfoliation of Graphitic Carbon Nitride for Enhanced Oxidative Desulfurization: A Facile and General Strategy. *ACS Sustainable Chem. Eng.* **2019**, *7*, 4941−4950.

(17) Fu, J.; Yu, J.; Jiang, C.; Cheng, B. G-C3N4-Based Heterostructured Photocatalysts. *Adv. Energy Mater.* **2018**, *8*, 1701503.

(18) Can, F.; Courtois, X.; Duprez, D. Tungsten-based Catalysts for Environmental Applications. *Catalysts* **2021**, *11*, 703.

(19) Kumar, R. D.; Andou, Y.; Karuppuchamy, S. Synthesis and Characterization of Nanostructured Ni-WO3 and NiWO4 for Supercapacitor Applications. *J. Alloys Compd.* **2016**, *654*, 349−356.

(20) Wang, Y.; Wang, Y.; Bai, J.; Duan, S.; Wang, R.; Lau, W. M. In-Situ Etching Synthesis of 3D Self-Supported Serrated Ni-WO3 for Oxygen Evolution Reaction. *J. Alloys Compd.* **2022**, *893*, 162134.

(21) Jossen, R.; Heine, M. C.; Pratsinis, S. E.; Augustine, S. M.; Akhtar, M. K. Thermal Stability and Catalytic Activity of Flame-Made Silica−Vanadia−Tungsten Oxide−Titania. *Appl. Catal. B* **2007**, *69*, 181−188.

(22) Nikolla, E.; Schwank, J.; Linic, S. Promotion of the Long-Term Stability of Reforming Ni Catalysts by Surface Alloying. *J. Catal.* **2007**, *250*, 85−93.

(23) Hameeda, B.; Mushtaq, A.; Saeed, M.; Munir, A.; Jabeen, U.; Waseem, A. Development of Cu-Doped NiO Nanoscale Material as Efficient Photocatalyst for Visible Light Dye Degradation. *Toxin Rev.* **2021**, *40*, 1396−1406.

(24) Molaei, P.; Rahimi-Moghadam, F. Porous G-C3N4 Nanosheets through Facile Thermal Polymerization of Melamine in the Air for Photocatalyst Application. *J. Mater. Sci.: Mater. Electron.* **2021**, *32*, 19655−19666.

(25) Zhang, W.; Zhou, L.; Deng, H. Ag Modified G-C3N4 Composites with Enhanced Visible-Light Photocatalytic Activity for Diclofenac Degradation. *J. Mol. Catal. A: Chem.* **2016**, *423*, 270−276.

(26) Ma, F.; Sun, C.; Shao, Y.; Wu, Y.; Huang, B.; Hao, X. One-Step Exfoliation and Fluorination of g-C3N4 Nanosheets with Enhanced Photocatalytic Activities. *New J. Chem.* **2017**, *41*, 3061−3067.

(27) Kaur, M.; Pal, K. Synthesis, Characterization and Electrochemical Evaluation of Hydrogen Storage Capacity of Graphitic Carbon Nitride and Its Nanocomposites in an Alkaline Environment. *J. Mater. Sci.: Mater. Electron.* **2021**, *32*, 12475−12489.

(28) Nguyen, H. T. T.; Truong, T. H.; Nguyen, T. D.; Dang, V. T.; Vu, T. V.; Nguyen, S. T.; Cu, X. P.; Nguyen, T. T. O. Ni-Doped WO3 Flakes-Based Sensor for Fast and Selective Detection of H2S. *J. Mater. Sci.: Mater. Electron.* **2020**, *31*, 12783−12795.

(29) Nithiyanantham, U.; Ede, S. R.; Anantharaj, S.; Kundu, S. Self-Assembled NiWO4 Nanoparticles into Chain-like Aggregates on DNA Scaffold with Pronounced Catalytic and Supercapacitor Activities. *Cryst. Growth Des.* **2015**, *15*, 673−686.

(30) Yang, J.; Chen, H.; Gao, J.; Yan, T.; Zhou, F.; Cui, S.; Bi, W. Synthesis of Fe3O4/g-C3N4 Nanocomposites and Their Application in the Photodegradation of 2,4,6-Trichlorophenol under Visible Light. *Mater. Lett.* **2016**, *164*, 183−189.

(31) Rezvani, M. A.; Maleki, Z. Facile Synthesis of Inorganic−Organic Fe2W18Fe4@NiO@CTS Hybrid Nanocatalyst Induced Efficient Performance in Oxidative Desulfurization of Real Fuel. *Appl. Organomet. Chem.* **2019**, *33*, No. e4895.

(32) Li, L.; Zhang, J.; Shen, C.; Wang, Y.; Luo, G. Oxidative Desulfurization of Model Fuels with Pure Nano-TiO2 as Catalyst Directly without UV Irradiation. *Fuel* **2016**, *167*, 9−16.

(33) Saeed, M.; Munir, M.; Nafees, M.; Shah, S. S. A.; Ullah, H.; Waseem, A. Synthesis, Characterization and Applications of Silylation Based Grafted Bentonites for the Removal of Sudan Dyes: Isothermal,

Kinetic and Thermodynamic Studies. *Microporous Mesoporous Mater.* **2020**, *291*, 109697.
(34) Tariq, S.; Saeed, M.; Zahid, U.; Munir, M.; Intisar, A.; Asad Riaz, M.; Riaz, A.; Waqas, M.; Abid, H. M. W. Green and Eco-Friendly Adsorption of Dyes with Organoclay: Isothermal, Kinetic and Thermodynamic Studies. *Toxin Rev.* **2021**, 1.
(35) Saeed, M.; Farooq, K.; Nafees, M.; Arshad, M.; Akhter, M. S.; Waseem, A. Green and Eco-Friendly Removal of Mycotoxins with Organo-Bentonites; Isothermal, Kinetic, and Thermodynamic Studies. *CLEA: Soil, Air, Water* **2020**, *48*, 1900427.
(36) Wei, S.; He, H.; Cheng, Y.; Yang, C.; Zeng, G.; Qiu, L. Performances, Kinetics and Mechanisms of Catalytic Oxidative Desulfurization from Oils. *RSC Adv.* **2016**, *6*, 103253−103269.
(37) Zuo, M.; Huang, X.; Li, J.; Chang, Q.; Duan, Y.; Yan, L.; Xiao, Z.; Mei, S.; Lu, S.; Yao, Y. Oxidative Desulfurization in Diesel via a Titanium Dioxide Triggered Thermocatalytic Mechanism. *Catal. Sci. Technol.* **2019**, *9*, 2923−2930.
(38) Chen, K.; Zhang, X. M.; Yang, X. F.; Jiao, M. G.; Zhou, Z.; Zhang, M. H.; Wang, D. H.; Bu, X. H. Electronic Structure of Heterojunction MoO2/g-C3N4 Catalyst for Oxidative Desulfurization. *Appl. Catal. B Environ.* **2018**, *238*, 263−273.
(39) Zhao, R.; Li, X.; Su, J.; Gao, X. Preparation of WO3/g-C3N4 Composites and Their Application in Oxidative Desulfurization. *Appl. Surf. Sci.* **2017**, *392*, 810−816.
(40) Chen, L.; Ren, J. T.; Yuan, Z. Y. Atomic Heterojunction-Induced Electron Interaction in P-Doped g-C3N4 Nanosheets Supported V-Based Nanocomposites for Enhanced Oxidative Desulfurization. *Chem. Eng. J.* **2020**, *387*, 124164.
(41) Xun, S.; Ti, Q.; Wu, L.; He, M.; Wang, C.; Chen, L.; Yang, W.; Zhu, L.; Zhu, W.; Li, H. Few Layer G-C3N4Dispersed Quaternary Phosphonium Ionic Liquid for Highly Efficient Catalytic Oxidative Desulfurization of Fuel. *Energy Fuels* **2020**, *34*, 12379−12387.
(42) Hou, L. P.; Zhao, R. X.; Li, X. P.; Gao, X. H. Preparation of MoO2/g-C3N4 Composites with a High Surface Area and Its Application in Deep Desulfurization from Model Oil. *Appl. Surf. Sci.* **2018**, *434*, 1200−1209.
(43) Hasannia, S.; Kazemeini, M.; Seif, A.; Rashidi, A. Oxidative Desulfurization of a Model Liquid Fuel over an RGO-Supported Transition Metal Modified WO3 Catalyst: Experimental and Theoretical Studies. *Sep. Purif. Technol.* **2021**, *269*, 118729.
(44) Shadmehri, M. A.; Housaindokht, M. R.; Nakhaei Pour, A. Oxidative Desulfurization of Dibenzothiophene via Layered Graphitic Carbon Nitride-Coordinated Transition Metal as a Catalyst. *New J. Chem.* **2021**, *45*, 16773−16783.

https://doi.org/10.1021/acsomega.2c00886
ACS Omega 2022, 7, 15809−15820